Chapter 5. A Numerical Optimization Method To Improve Materials Characterization

5.1 Thickness Effect on Dual-Energy Transmission Imaging

5.1.1 Thickness effect on transmission imaging

The straightforward strategy for x-ray image analysis uses the intensities of regions in the image as a means of identification: it is assumed that each region corresponds to an object and the same type of material will have the same intensity. If this intensity is different from that of others or can be made so by image processing and sensor fusion, then it can be used to characterize materials.

But the application of this approach is seriously restricted by several factors: (1) a material's location in the field of view; (2) its orientation; and (3) its thickness.

The thickness is not an intrinsic property of the material, and this represents a major problem. We will show later in this section that a change of the material's appearance in the field of view and its orientation do nothing but cause a variation of the pass-through thickness of x-rays. Figure 5.1-1 gives a transmission image for plastic wedges at the energy of 75 keV, and their corresponding image intensity levels (also called gray levels). It can be seen that the

transmission is approximately exponentially attenuated with the thickness of material, as expected.

5.1.2 Effect of the material's appearing in the field of view

As described in Chapter 3, the "flying spot" imaging techniques are used in the prototype scanner. A rotating chopper wheel and a stationary slit form a thin pencil beam of x-ray radiation that is used to raster scan a bag. A single detector collects the transmitted radiation and converts it to an electrical signal. This signal is digitized, stored and used to create a visual image of the transmission of x-rays through the bag [SCH91].

But this approach is not without pitfalls, as is any x-ray imaging system that uses a fan-beam of x-rays. When the beam of x-rays is chopped up and down, the corresponding thickness passed through a certain material by the beam of x-rays will be changed (see Figure 5.1-2).

From the figure above, we see that the real pass-through thickness of x-rays, t, is associated with its incident angle θ,

$$t = t_0 \sec(\theta) \tag{5.1}$$

where t_0 is the material thickness which is defined as the measurement of the object in the direction normal to the vertical detector plane.

It is known from Equation (5.1) that the thickness variation is in proportion to the material thickness t_0 for a certain incidence angle θ. Figure 5.1-3 gives an example with θ changed from 0 to 50 degrees.

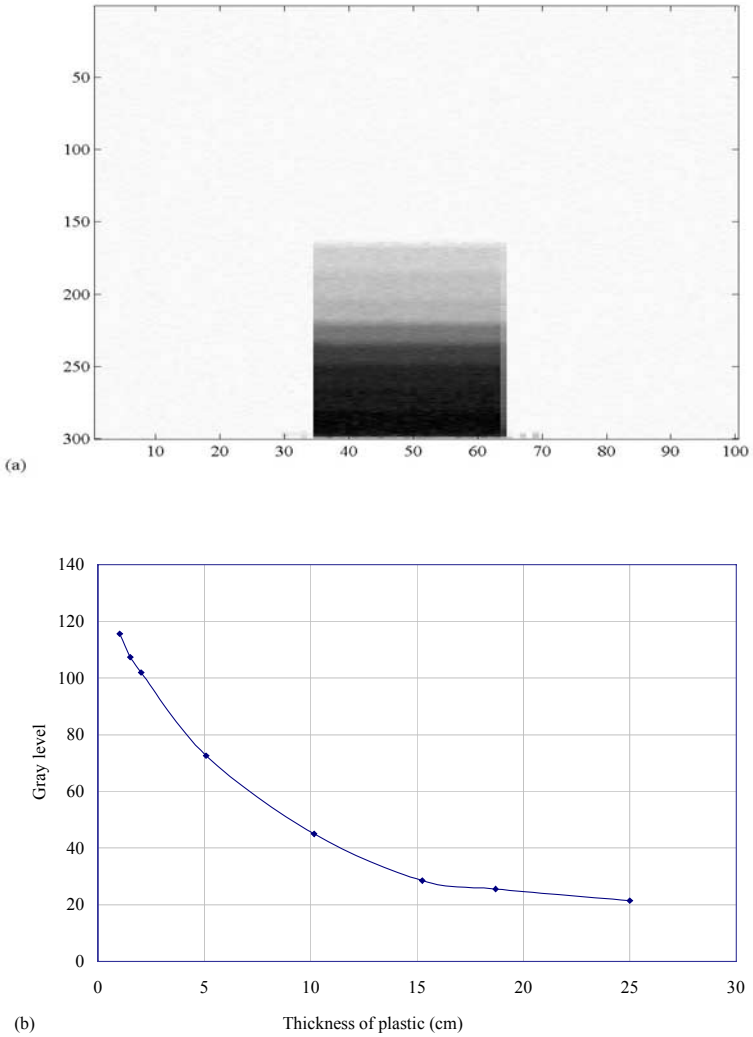

Figure 5.1-1 An example of the thickness effect on transmission imaging: (a) transmission image of plastic wedges, (b) representative gray levels corresponding to each step.

If $\theta = 0$, which corresponds to the material placed at the bottom of the bag, $(t - t_0)/t_0$ will be equal to 0. It means the pass-through thickness is the same as the material thickness. Otherwise, the upper the material in the view of field, the bigger the difference between t and t_0. When the incident angle is 50 degrees, the pass-through thickness is as 1.6 times big as the material thickness. Therefore, the position variation of the object results in the variation of the incidence angles, then the pass-through thickness, and finally the transmission imaging intensity. A measurement for plastic plates of thickness 2.5 cm and 15 cm is given in Figure 5.1-4.

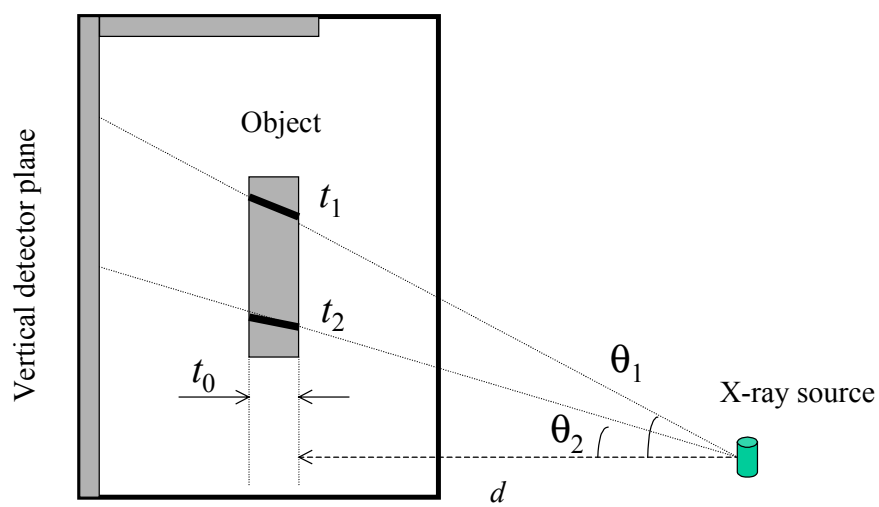

Figure 5.1-2 Schematic descriptions of material's appearance in the field of view.

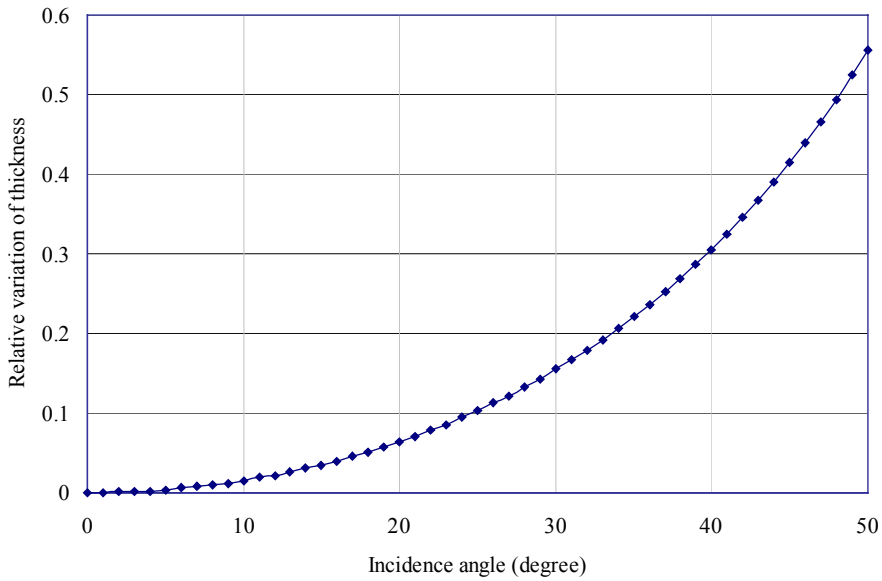

Figure 5.1-3 Relative variation of pass-through thickness versus the incidence angle for an object placed perpendicularly on conveyer belt.

Two conclusions can be verified from the figure. 1) Increasing the thickness will increase the variation of the received signal intensity. The maximum variations of 2.5 cm and 15 cm plastic plates are about seven percent and thirty percent respectively. 2) Increasing the incidence angle will therefore increase the variation of the transmitted signal intensity assuming that the object is oriented vertically. For example, the variation at row 150 (with $\theta \approx 22.3^\circ$) is about fourteen percent, but it increases to thirty percent at row 350 (with $\theta \approx 39.4^\circ$).

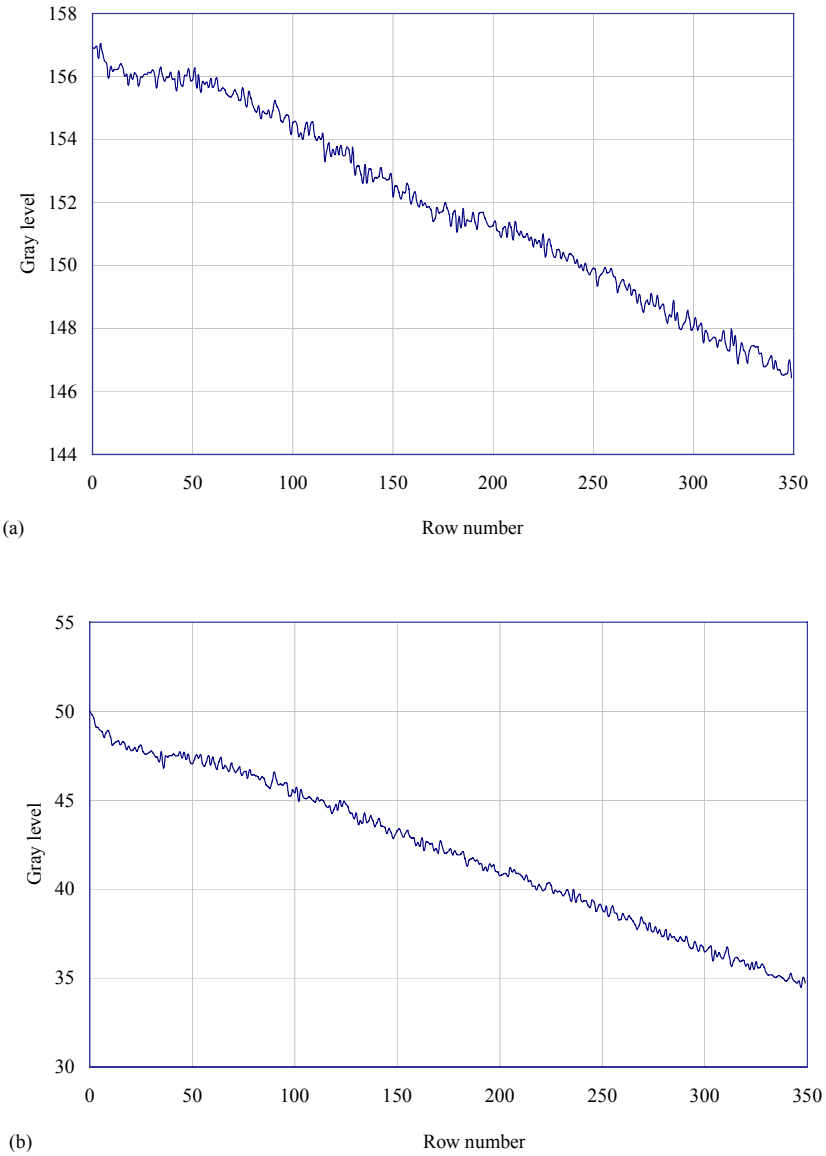

Figure 5.1-4 Variation of the received signal intensity due to material's location (given as row number) in the field of view: (a) plastic plate of 2.5 cm, (b) plastic plate of 15 cm. The materials are placed vertically on conveyer belt, similar to the diagram in Figure 5.1-2.

5.1.3 Effect of the material orientation

The material can be randomly placed in a luggage bag. Therefore, a material's location in the field of view is undetermined when the bag is scanned through x-ray machine. This means that a certain object may have different transmission signal intensity.

In addition to a material appearing randomly in the field of view, it may also have any orientation (see Figure 5.1-5), which will affect intensity of the transmitted signal too. Under such a circumstance, the pass-through thickness of x-ray can be expressed as,

$$t = t_0 \, {\sin(180-\alpha)}/{\sin(a-\theta)} \tag{5.2}$$

where α is a measurement of the object orientation, the other parameters have the same meanings as in Equation (5.1).

Equation (5.1) is a particular case of Equation (5.2) with α = 90^0. A typical example measured on the plastic plate of 2.5 cm with an orientation of 68 degree and 126 degree is given in Figure 5.1-6. It ban be seen that the material orientation has an effect on the transmitted signal intensity too, and makes the real measurements more complicated. The maximum variations of intensities are about 23% and –5% for α = 68° and α = 126°, respectively.

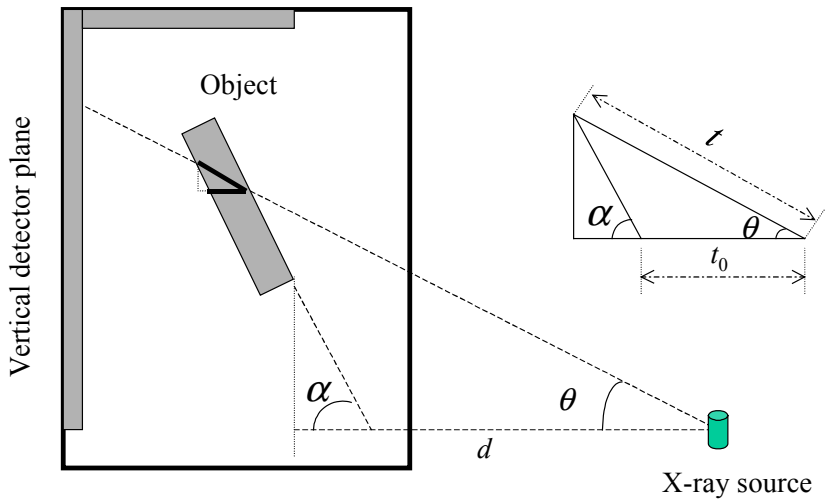

Figure 5.1-5 Schematic description of material orientation.

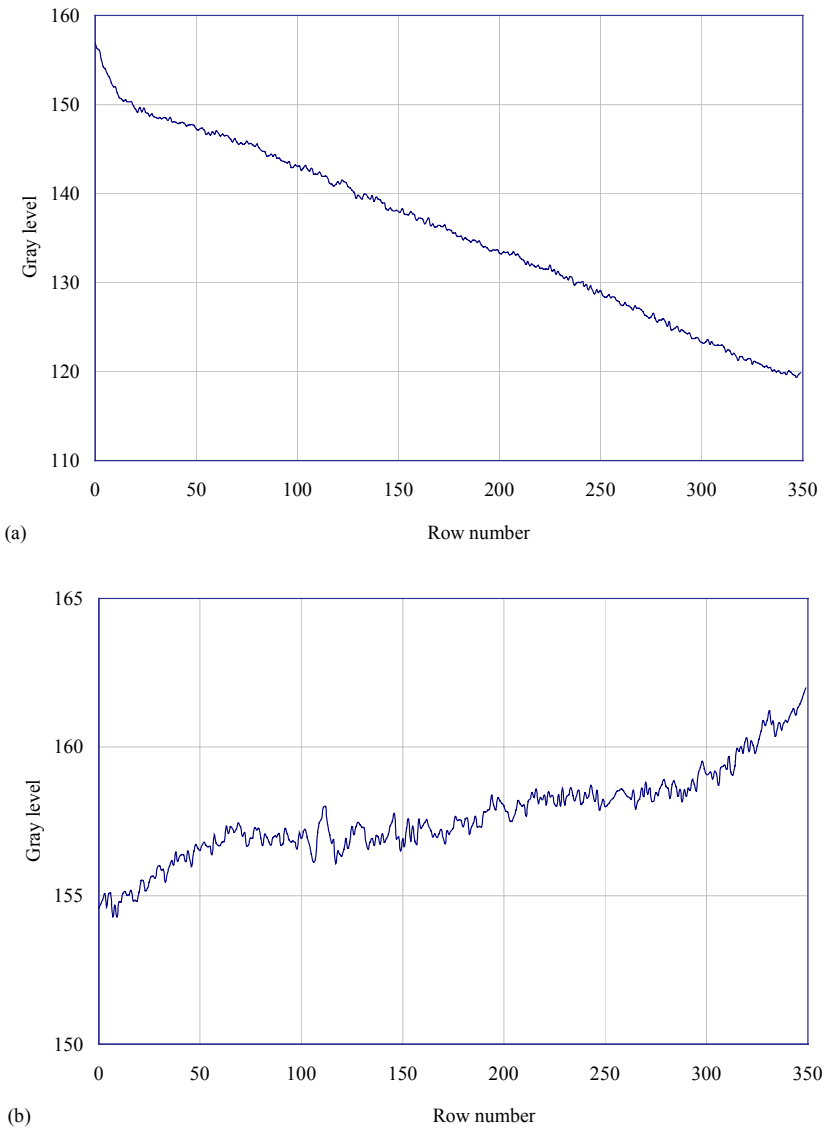

Figure 5.1-6 Variation of the transmitted signal intensity versus the incidence angles (given as row number) with different orientation: (a) $\alpha = 68^{o}$, (b) $\alpha = 126^{o}$.

5.1.4 Thickness effect on dual-energy transmission imaging

As described in Chapter 3, the total transmitted signal for a certain input energy E_{in} is the integration of the transmitted signal at all energies as long as the x-ray source spectrum is not monochromatic. For the convenience of discussion, we rewrite the detected transmission signal again,

$$T(x, y) = \int_0^{E_{in}} N(E)\, e^{-\left\{\int dz' \mu_t^*(x', y', z', E)\, \rho(x', y', z')\right\}} P_d(E)\, E\, dE \tag{5.3}$$

For the simple object having a total linear attenuation coefficient $\mu_t(x', y', E)$ and thickness t, the Equation (5.3) becomes,

$$T(x, y) = \int_0^{E_{in}} N(E)\, e^{-\mu_t(x', y', E)t}\, P_d(E)\, E\, dE \tag{5.4}$$

For any measurement on an object at location (x, y) in the image, our goal here is to analyze the relationship between transmission intensity and object thickness for a given energy spectrum. Therefore we remove the spatial coordinate from Equation (5.4), and this yields,

$$T = \int_0^{E_{in}} N(E) E P_d(E) e^{-\mu_t(E)t} dE \tag{5.5}$$

From Equation (5.5), we know that the total transmission signal has a dependence on the thickness of materials.

The dual energy x-ray imaging system ideally is immune to changes in material thickness. But the application always fails due to the use of the polychromatic spectrum of the x-ray source. Let two input energies be E_H and E_L, then for a certain material we have,

$$\left.\begin{aligned} T_H &= \int_0^{E_H} N(E)EP_d(E)e^{-\mu_t(E)t}dE \\ T_L &= \int_0^{E_L} N(E)EP_d(E)e^{-\mu_t(E)t}dE \end{aligned}\right\} \tag{5.6}$$

Currently, dual energy x-ray imaging systems use a measurement which is formulated by combining T_H and T_L as,

$$R = \frac{\log(T_L/T_{L0})}{\log(T_H/T_{H0})} \tag{5.7}$$

where R is called the dual energy, T_{H0} and T_{L0} are the transmission signals at high energy and low energy obtained in free space. Because of the integration operation, it is impossible to remove the thickness t from the equation above. That is to say, R is not only related to the material atomic number Z, atomic weight A, and density ρ, but is also related to material thickness t.

To show this thickness dependence, the measurements on three step wedges (aluminum, white plastic, and clear plastic) at low energy (with 75 keV as a maximum input voltage) and high energy (with 145 keV as a maximum input voltage) are given in Figures 5.1-7, 5.1-8 and 5.1-9. Their transmission signal intensities, T_L and T_H for low and high energies respectively, and corresponding dual energy value, R, for each step are given in Tables 5.1-1, 5.1-2, and 5.1-3.

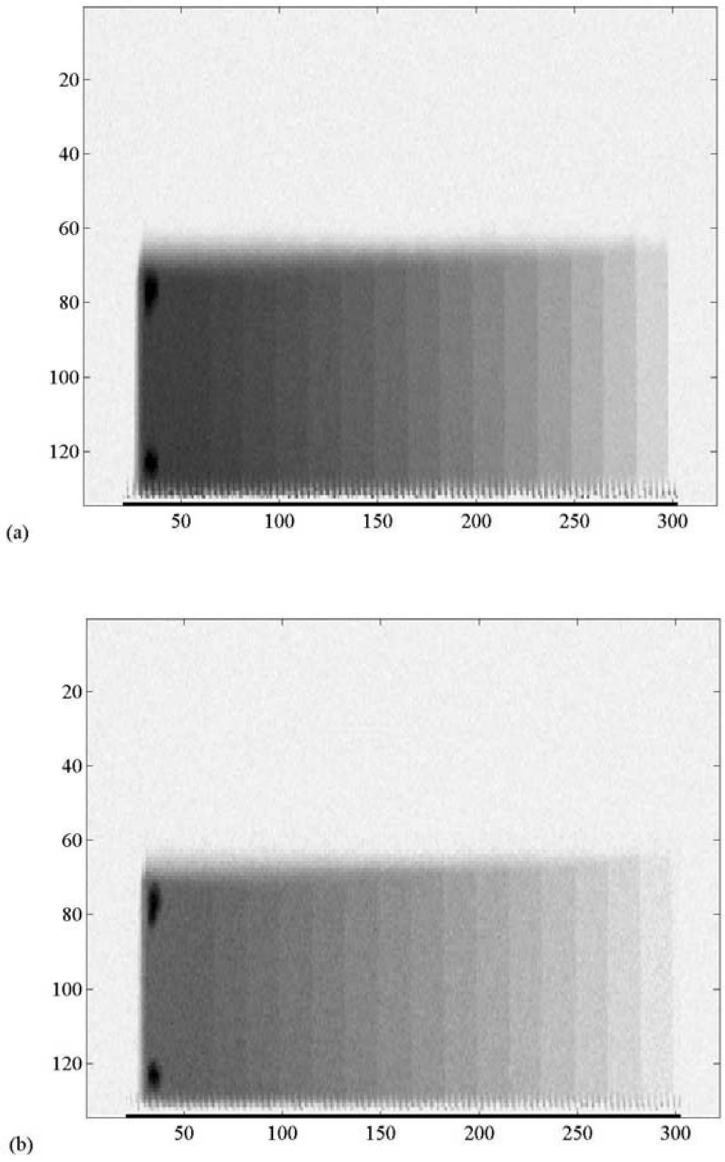

Figure 5.1-7 White plastic step wedge scanned at: (a) 75 keV; (b) 150 keV.

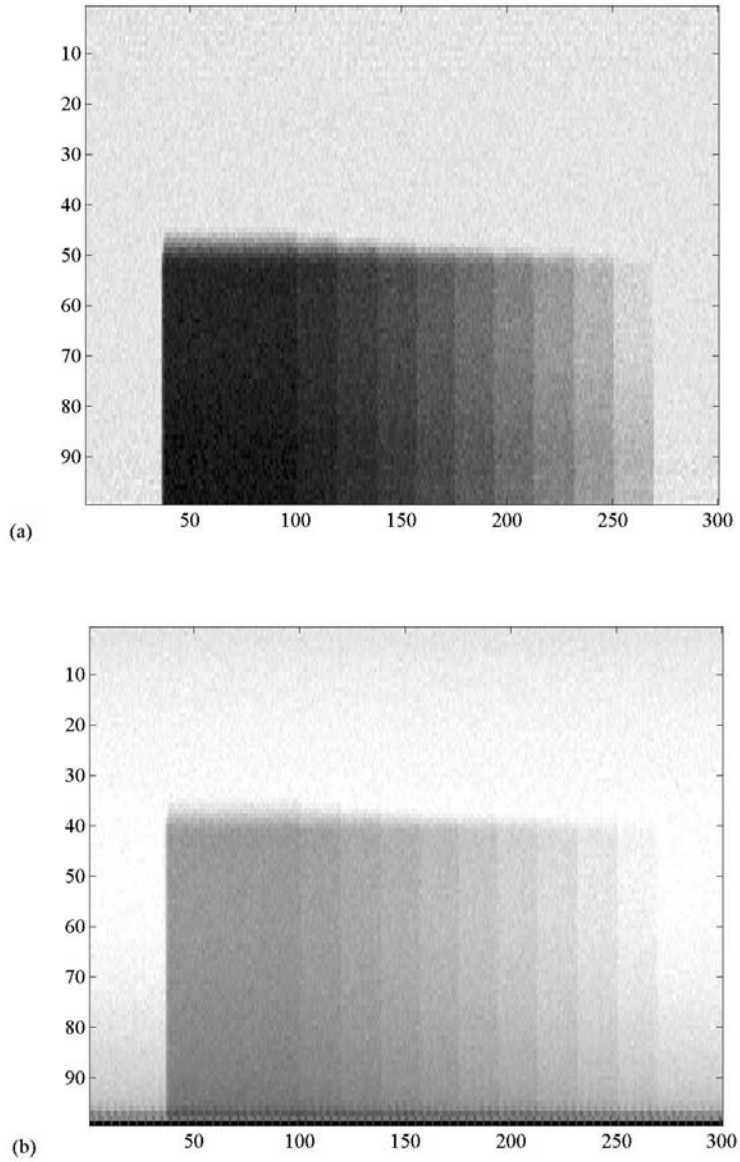

Figure 5.1-8 Clear plastic step wedge scanned at: (a) 75 keV; (b) 150 keV.

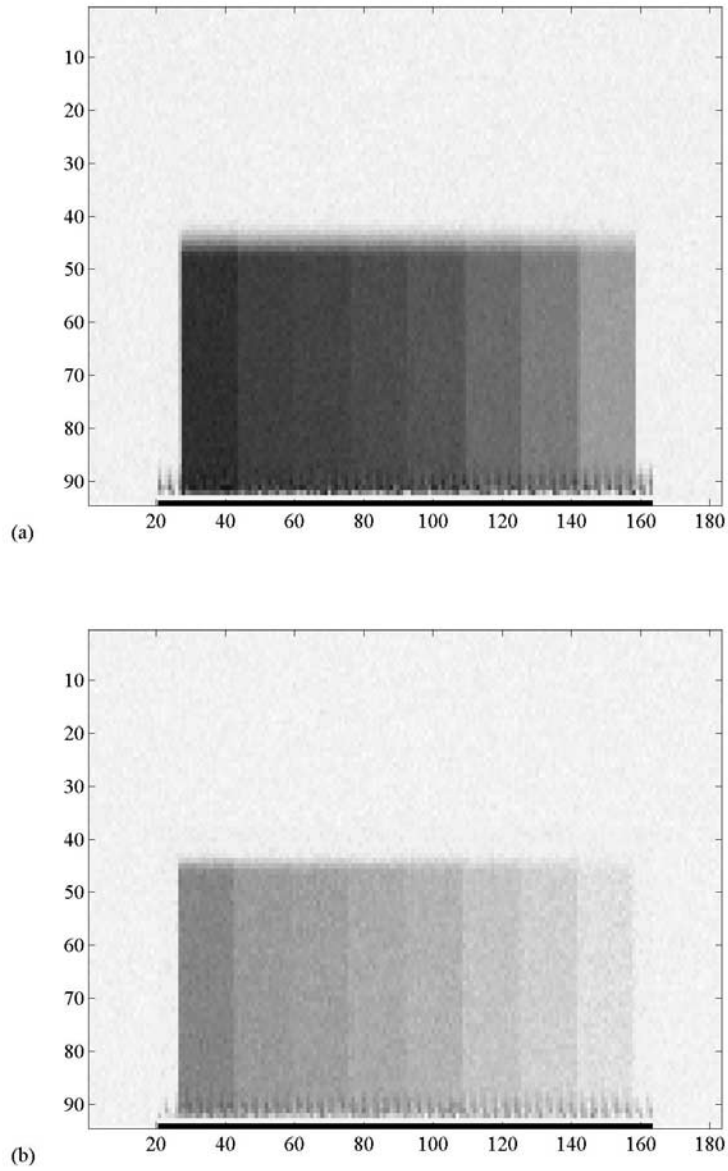

Figure 5.1-9 Aluminum step wedge scanned at: (a) 75 keV; (b) 150 keV.

Table 5.1-1 Transmission signals and dual energy values obtained from the prototype scanner for aluminum step wedge.

Thickness (cm)	T_H	T_L	R
0.259	179.4964	139.2806	5.9616
0.508	167.0863	112.9496	4.3907
0.711	158.1295	98.0576	3.8715
1.014	146.0432	81.2230	3.4340
1.189	139.2446	73.2374	3.2463
1.392	131.7986	66.1151	3.0438
1.524	127.4820	62.0144	2.9525
2.032	111.7266	48.4173	2.6900
Mean			3.6988
Standard deviation			1.0628

Table 5.1-2 Transmitted signals and their dual energies obtained from the prototype scanner for white plastic step wedge.

Thickness (cm)	T_H	T_L	R
0.635	177.8417	181.3909	2.1520
1.27	168.6331	164.6043	1.9886
1.905	159.7122	150.6954	1.8651
2.54	151.0791	138.7050	1.7691
3.175	142.5899	127.6739	1.6981
3.81	135.2518	117.8417	1.6687
4.445	128.2014	108.9688	1.6396
5.08	121.1511	100.8153	1.6053
5.715	114.3885	92.9017	1.5842
6.35	108.3453	86.1871	1.5642
6.985	102.7338	79.9520	1.5507
7.62	97.1223	74.1966	1.5319
8.255	91.6547	68.6811	1.5158
8.89	86.9065	63.8849	1.5051
9.525	82.1583	59.0887	1.4972
Mean			1.6757
Standard deviation			0.1927

Table 5.1-3 Transmission signals and dual energy values obtained from the prototype scanner for clear plastic step wedge.

Thickness (cm)	T_H	T_L	R
0.635	178.1775	176.6427	2.6352
1.27	168.5851	158.4173	2.2965
1.905	160.1918	144.9880	2.1173
2.54	151.3189	132.1343	1.9892
3.175	143.6451	121.3909	1.9196
3.81	136.2110	111.4149	1.8692
4.445	128.5372	102.3981	1.8061
5.08	122.0624	94.5324	1.7750
5.715	114.8273	86.6667	1.7312
6.35	109.8321	80.7194	1.7202
Mean			1.9859
Standard deviation			0.2917

From the above tables we see that dual energy values take a big change if the thickness of material is varied. For example, it is changed from 5.96 to 2.69 when thickness increases from 0.259 cm to 2.032 cm for the aluminum step wedge. Obviously this will degrade the material characterization due to the following reasons:

- The same material might have different R values if different thickness are applied. For example, R values are 2.6 and 1.7 for clear plastic having thickness of 0.635 cm and 6.35 cm, respectively.
- The different materials, characterized by μ_1 and μ_2, may have the same R values if thickness of materials meets $\mu_1 t_1 = \mu_2 t_2$. The clear plastic of 5.1 cm, for example, will have the same dual energy as white plastic of 2.5 cm.

5.2 A Numerical Method To Overcome The Thickness Effect

To overcome the effect of thickness, a numerical method is proposed and developed. This numerical method not only improves materials characterization, but also provides a new design methodology for the dual-energy x-ray imaging systems.

5.2.1 Numerical expression of the transmission signal

For a given x-ray source and detector, the number of the incident x-ray photons $N(E)$, x-ray photon's energy E, and the detection probability of a photon $P_d(E)$ in Equation (5.6) are either known parameters or available through simulations. Let $K(E) = N(E)EP_d(E)$, the transmission signal T at a certain spot can be written as,

$$T = \int_0^{E_{in}} K(E) e^{-\mu_t(E)t} dE \tag{5.8}$$

The integrand, $K(E)$, is assumed to be known only at discrete points, so a numerical integration method is needed for the approximate evaluation of this finite integral.

(1) Composite quadrature rule

The integral over a finite interval [0, E_{in}] can be computed numerically by breaking it into small pieces. In particular, the area under the function curve is broken into narrow strips determined by some partition of the interval of integration [SKE93],

$$0 = E_0 < E_1 < \cdots < E_M = E_{in}$$

How to choose the partition is a difficult question. One may select different partition sizes, one may use Newton-Cotes formula by interpolating functions at equidistant points and integrate the interpolated polynomial, or one may use the Gaussian quadrature formula to which non-equidistant interpolation points are applied [KRE98] [GHI70]. Once a partition has been determined, Equation (5.8) can be rewritten as,

$$T = \int_0^{E_{in}} f(E) dE = \int_{E_0}^{E_1} f(E) dE + \int_{E_1}^{E_2} f(E) dE + \cdots + \int_{E_{M-1}}^{E_M} f(E) dE \tag{5.9}$$

where $f(E) = K(E) e^{-\mu_t(E)t}$.

By using some simple rules to approximate each of the integrals on the right, the integral over total interval can be estimated. The repeated use of a simple rule in this way is often called a composite rule (see Figure 5.2-1) [SKE93].

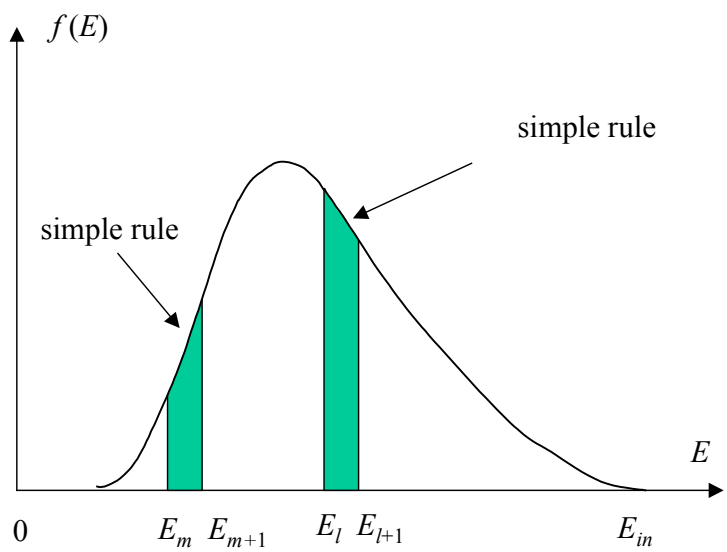

Figure 5.2-1 Composite rule as a sum of simple rules.

(2) Simpson rule

The Simpson rule, one of the simple rules, is most frequently used in numerical integration [DAV67].

The Simpson rule approximates an integral by the area as a width multiplied by a weighted average of integrands from left, center, and right with a full two-thirds of the weight on the center value,

$$\int_{E_m}^{E_{m+1}} f(E)dE = h\left[\frac{1}{6}f(E_m)+\frac{2}{3}f(\frac{E_m+E_{m+1}}{2})+\frac{1}{6}f(E_{m+1})\right]+\xi(f) \tag{5.10}$$

where $h = E_{m+1} - E_m$, and $\xi(f) = -\frac{\left(h/2\right)^5}{90} f^{(4)}(\eta)$ is the expected error [JOH82].

If equal subintervals are used in Equation (5.10), the composite rule as a sum of Simpson rules will be [DAV67],

$$T \approx \frac{h}{6}\left[f(E_0)+f(E_M)+2\sum_{m=1}^{M/2} f(E_0+2(m-1)h)+4\sum_{m=1}^{M/2} f(E_0+(2m-1)h)\right]$$

for M = even number, (5.11a)

$$T \approx \frac{h}{6}\left[f(E_0)+f(E_M)+2\sum_{m=1}^{M-1/2} f(E_0+2mh)+4\sum_{m=1}^{M-1/2} f(E_0+(2m-1)h)\right]$$

for M = odd number, (5.11b)

where $M = E_{in}/h$ is the number of intervals. The error is the sum of the errors on each interval and so [JOH82],

$$\xi_M(f) = -\frac{\left(h/2\right)^4 E_{in}}{180} f^{(4)}(\eta) \tag{5.12}$$

In general, we can write Equation (5.11) in the form of,

$$T \approx \sum_{m=0}^{M} a_m e^{-\psi_m} \tag{5.13}$$

where

$$a_m = \begin{cases} \frac{h}{6} K(E_0), \text{ for } m = 0 \\ \frac{h}{3} K(E_m), \text{ for } 0 < m < M \text{ and } m \text{ is an even number} \\ \frac{2h}{3} K(E_m), \text{ for } 0 < m < M \text{ and } m \text{ is an odd number} \\ \frac{h}{6} K(E_M), \text{ for } m = M \end{cases} \tag{5.14}$$

and

$$\psi_m = \mu_t(E_m)t \tag{5.15}$$

It should be noted that we are not going to calculate total transmission signal T with Equation (5.13). On the contrary, we will only estimate the area attenuation parameter ψ_m at particular energy levels E_m with the measured value T.

5.2.2 Solving equations with numerical optimization

Although it is impossible to solve Equation (5.13) for ψ_m directly, we can make a best estimation. By defining an objective function, $\varepsilon(\psi)=\left[T-\sum_{m=0}^{M} a_m e^{-\psi_m}\right]^2$, the problem can be mathematically described as,

$$\text{Given} \quad \varepsilon(\psi)=\left(T-\sum_{m=0}^{M} a_m e^{-\psi_m}\right)^2, \quad \text{find} \quad \psi^* = \{\psi_0, \psi_1, \ldots, \psi_M\}, \quad \text{for which } \varepsilon \text{ is minimized.} \tag{5.16}$$

Equation (5.16) is a typical problem in optimization. Some a priori knowledge on the relationship between cross-sections and energy levels (Equations 2.6, 2.8, and 2.9) were used as constraints to (5.16). As known in Section 2.2, only one cross-section plays a significant role in a certain energy region. We therefore managed to use each cross-section separately, yielding the constraints given in (5.17). The first constraint in (5.17) is straightforward; we will take (2.6) as an example to explain formulation of the second constraint in (5.17).

From (2.6) we know $\sigma_{pe}(E_m) \approx 10\frac{Z^{4.5}}{E_m^3}$ and $\sigma_{pe}(E_n) \approx 10\frac{Z^{4.5}}{E_n^3}$; this results in $\sigma_{pe}(E_m)\cdot E_m^3 = \sigma_{pe}(E_n)\cdot E_n^3$. It is also known that ψ_m is proportional to μ_m from (5.15), and μ_m is in proportion to $\sigma_{pe}(E_m)$ from (2.13) (we have supposed there is only photo-electric effect in the region of low energy), we therefore obtain the second constraint in (5.17).

$$\left.\begin{array}{l} \psi_0 \geq \psi_1 \geq \cdots \geq \psi_M \geq 0 \\ \psi_m E_m^3 = \psi_{m+1} E_{m+1}^3 \ \text{ for } m \leq M_1 \\ \psi_m E_m^2 = \psi_{m+1} E_{m+1}^2 \ \text{ for } M_1 < m \leq M_2 \\ \psi_m = \psi_{m+1} \ \text{ for } M_2 < m \leq M \end{array}\right\} \tag{5.17}$$

where M_1 and M_2 are two particular values to define the region of energy levels. In this research, $M_1 = 5$ and $M_2 = 15$ were selected empirically when M is equal to 31 with input voltage of 145 keV and equally interval voltage of 5 keV.

The optimization toolbox produced by the MathWorks, Inc., which uses sequential quadratic programming (SQP) method, provides a way to find a solution to our problem defined in (5.16) subject to constraints in (5.17). In this method, a quadratic programming subproblem is solved at each iteration, and an estimation of the Hessian of the Lagrangian is updated at each iteration using the BFGS formula [BRO70] [FLE70] [GOL70] [SHA70]. More description on the algorithms used in the optimization toolbox can be found in [COL96].

5.3 Implementation

From the results discussed in previous section, the numerical method is summarized as follows:

- *Algorithm 5.1*

  (i) Input the coefficients $\{a_m\}$ in Equation (5.14);

  (ii) Input each object's intensity (gray level) at low and high energy, T_L, T_H;

  (iii) Let $T = T_L$, solving Equation (5.16) for ψ_m, $m = \{0, 1, 2, \ldots, M\}$;

  (iv) Let $T = T_H$, and solving Equation (5.16) for ψ_n, $n = \{0, 1, 2, \ldots, N\}$.

  (v) Calculate dual-energy by using $R = \psi_i / \psi_j$, where ψ_i is the area attenuation at particular energy E_i while low energy is applied, and ψ_j is the area attenuation at particular energy E_j while high energy is applied.

The MATLAB optimization toolbox was used to implement step (iii) and step (iv).

5.4 Application Examples

This section gives some examples of this method. Two energy levels used to calculate R in Algorithm 5.1, E_i, E_j, were selected based on the following concerns:

- To get a better dual-energy effect, two energies should be separated as much as possible;
- Low energy x-rays have poor penetration on thicker objects, while practical systems restrict the choice of the high energy level;
- Based on these considerations and on simulation results, the low energy level is often chosen to lie in the range 30 ~ 60 keV, and the high energy level is often chosen to be 80 ~ 110 keV [GRO91].

Cases 1 to 6, shown in Tables 5.4-1 to 5.4-6, give the results for plastic plates with various situations, such as positions in the field of view, orientations, and different thickness. We use 30 keV and 95 keV to calculate dual-energy values. The results for three step wedges are given in Cases 7 to 9, where 40 keV and 105 keV are used to calculate dual-energy in these three cases.

By comparing these tables with Tables 5.1-1 to 5.1-3, it is seen that dual-energy calculated by using the numerical optimization method falls into a small region, no matter where an object is located, what its orientation is, and what its thickness is. For now, it is only important to know that the mean values and standard deviations are changed for three step wedges. In next section, we will analyze the effect of this variation on material characterization by using parametric method.

Table 5.4-1 Dual energy for white plastic plate of 2.54 cm with $\alpha = 0^{o}$.

Image row number	Incident angle	Pass-through thickness	Dual energy $R = \psi(30\,\text{keV})/\psi(95\,\text{keV})$
0	0.0	2.54	1.8089
50	9.5	2.58	1.7940
100	16.6	2.65	1.7666
150	22.3	2.75	1.8111
200	27.1	2.85	1.7344
250	31.4	2.97	1.7342
300	35.4	3.12	1.8228
Mean			1.7817
Standard deviation			0.0369

Table 5.4-2 Dual energy for white plastic plate of 5.08 cm with $\alpha = 0^{o}$.

Image row number	Incident angle	Pass-through thickness	Dual energy $R = \psi(30\,\text{keV})/\psi(95\,\text{keV})$
0	0.0	5.08	1.8334
50	9.5	5.15	1.7871
100	16.6	5.30	1.7885
150	22.3	5.49	1.8071
200	27.1	5.71	1.7742
250	31.4	5.95	1.7486
300	35.4	6.23	1.7234
Mean			1.7803
Standard deviation			0.0364

Table 5.4-3 Dual energy for white plastic plate of 15.24 cm with $\alpha = 0^{o}$.

Image row number	Incident angle	Pass-through thickness	Dual energy $R = \psi(30\text{ keV})/\psi(95\text{ keV})$
0	0.0	15.2	1.8030
50	9.5	15.5	1.7304
100	16.6	15.9	1.7513
150	22.3	16.5	1.7632
200	27.1	17.1	1.8465
250	31.4	17.8	1.7182
300	35.4	18.7	1.7675
Mean			1.7686
Standard deviation			0.0439

Table 5.4-4 Dual energy for white plastic plate of 2.54 cm with $\alpha = 68^{o}$.

Image row number	Incident angle	Pass-through thickness	Dual energy $R = \psi(30\text{ keV})/\psi(95\text{ keV})$
0	0.0	2.74	1.7386
50	9.5	2.98	1.7924
100	16.6	3.25	1.8152
150	22.3	3.55	1.7405
200	27.1	3.88	1.8579
250	31.4	4.26	1.7406
300	35.4	4.71	1.7353
Mean			1.7801
Standard deviation			0.0453

Table 5.4-5 Dual energy for white plastic plate of 2.54 cm with $\alpha = 126^{o}$.

Image row number	Incident angle	Pass-through thickness	Dual energy $R = \psi(30\,\text{keV})/\psi(95\,\text{keV})$
0	0.0	3.14	1.7909
50	9.5	2.84	1.7634
100	16.6	2.69	1.7193
150	22.3	2.61	1.7400
200	27.1	2.57	1.7543
250	31.4	2.55	1.7320
300	35.4	2.54	1.8308
Mean			1.7615
Standard deviation			0.0384

Table 5.4-6 Dual energy for white plastic plate of 5.08 cm with $\alpha = 68^{o}$.

Image row number	Incident angle	Pass-through thickness	Dual energy $R = \psi(30\,\text{keV})/\psi(95\,\text{keV})$
0	0.0	5.48	1.7436
50	9.5	5.96	1.8158
100	16.6	6.50	1.8088
150	22.3	7.10	1.8645
200	27.1	7.75	1.7237
250	31.4	8.51	1.7620
300	35.4	9.43	1.7689
Mean			1.7839
Standard deviation			0.0485

Table 5.4-7 Dual energy for white plastic step wedge.

Thickness (cm)	T_H	T_L	$R = \psi(40\,\text{keV})/\psi(105\,\text{keV})$
0.635	177.8417	181.3909	1.0768
1.27	168.6331	164.6043	1.1154
1.905	159.7122	150.6954	1.0610
2.54	151.0791	138.7050	1.0657
3.175	142.5899	127.6739	1.0364
3.81	135.2518	117.8417	1.0684
4.445	128.2014	108.9688	1.0762
5.08	121.1511	100.8153	1.0794
5.715	114.3885	92.9017	1.1297
6.35	108.3453	86.1871	1.1399
6.985	102.7338	79.9520	1.0711
7.62	97.1223	74.1966	1.0951
8.255	91.6547	68.6811	1.0475
8.89	86.9065	63.8849	1.1032
9.525	82.1583	59.0887	1.0764
Mean			1.0828
Standard deviation			0.0289

Table 5.4-8 Dual energy for clear plastic step wedge.

Thickness (cm)	T_H	T_L	$R = \psi(40\,\text{keV})/\psi(105\,\text{keV})$
0.635	178.1775	176.6427	1.3554
1.27	168.5851	158.4173	1.2736
1.905	160.1918	144.9880	1.2747
2.54	151.3189	132.1343	1.2392
3.175	143.6451	121.3909	1.2251
3.81	136.2110	111.4149	1.3052
4.445	128.5372	102.3981	1.2521
5.08	122.0624	94.5324	1.2275
5.715	114.8273	86.6667	1.2875
6.35	109.8321	80.7194	1.2651
Mean			1.2705
Standard deviation			0.0394

Table 5.4-9 Dual energy for aluminum step wedge.

Thickness (cm)	T_H	T_L	$R = \psi(40\,\text{keV})/\psi(105\,\text{keV})$
0.259	179.4964	139.2806	2.9188
0.508	167.0863	112.9496	2.9356
0.711	158.1295	98.0576	2.8762
1.014	146.0432	81.2230	2.9487
1.189	139.2446	73.2374	2.8235
1.392	131.7986	66.1151	2.9302
1.524	127.4820	62.0144	2.9543
2.032	111.7266	48.4173	2.8164
Mean			2.9005
Standard deviation			0.0551

5.5 Improvement Evaluation

5.5.1 Description of decision rule

The numerical optimization method calculates dual-energy values for two particular energy levels, thus making it possible to reduce thickness effect on material characterization. Now it is time to evaluate the system improvement that results by using the copper filter and the numerical method. Our comparison will focus on an estimation of the probability of error by using dual-energy information as a classification feature, x, with three step wedges. Under this circumstance, Bayes decision rule for minimizing the probability of error is [DUD73]: decide C_i if $P(C_i \mid x) > P(C_j \mid x)$, where $P(C_i \mid x)$ is called the a posteriori probability of class C_i given an observation x.

To evaluate the improvement analytically, we also need to estimate the probability density function of dual-energy measurements. Some assumptions are helpful for us to select a proper model:

- Materials appearing in luggage bags are independent from person to person;
- Materials inside a certain luggage bag are usually independent from each other;
- For a certain luggage bag, the position, thickness and orientation of each material are random.

All of the above factors affect the transmission signal intensity and therefore the dual-energy computation. Base on the above assumptions, we will use normal distribution as the probability density function. Thus, the decision rule above can be simplified as: decide C_i if

$$g_i(x) = -\frac{(x-\mu_i)^2}{2\sigma_i^2} + \log(P(C_i)) > g_j(x) \tag{5.29}$$

where $g_i(x)$ is called the discriminant function, $P(C_i)$ is the a priori probability of class C_i being present, and μ_i and σ_i^2 are the mean and variance of observations belonging to class C_i [DUD73]. If the a priori probabilities $P(C_i)$ are the same for all classes, above decision rule can be further simplified as: decide class C_i if

$$g_i(x) = -\frac{(x-\mu_i)^2}{2\sigma_i^2} > g_j(x) \tag{5.30}$$

We will give a comparison of the probability of error based on this decision rule.

5.5.2 Comparison of the probability of error

In Section 4.4, the dual-energy values for three step wedges without the copper filter were calculated (using the same equation as (5.7)) and given in three tables (Tables 4.4-1 to 4.4-3). The maximum input voltages at low and high energy are 75 keV and 145 keV respectively. In Section 5.4, the dual-energy values for the same wedges were obtained by using the numerical optimization method with the copper filter. Now we will evaluate the difference between them with respect to the probability of error. For convenience, their first and second moments are summarized in Table 5.5-1. The variance in the table, σ^2, is estimated with square of standard deviation due to the normal distribution assumption, i.e.,

$$\sigma^2 = \frac{1}{N-1}\sum_{i=1}^{N}(R_i - \mu)^2 \tag{5.31}$$

where N is the number of measurements, and R_i is the dual-energy for measurement i.

Table 5.5-1 Summary of dual-energy moments for three step wedges.

Class number i	Material	Dual-energy computed with $R = \frac{\log(T_L/T_{L0})}{\log(T_H/T_{H0})}$		Dual-energy obtained from the numerical method $R = \frac{\psi(40\text{ keV})}{\psi(105\text{ keV})}$	
		μ_i	σ_i^2	μ_i	σ_i^2
1	White plastic	1.2159	0.0074	1.0828	0.0008
2	Clear plastic	1.4647	0.0130	1.2705	0.0016
3	Aluminum	1.6691	0.0221	2.9005	0.0030

The probability density functions of dual-energy measurements for three step wedges are shown in Figure 5.5-1. Through further data analysis, we know that $g_1(1.3341) = g_2(1.3341)$ and $g_2(1.5760) = g_3(1.5760)$. By using the decision rule in (5.30), we classify the step wedges with the following distinct boundary: decide C_3 (i.e., aluminum) if $x > 1.5760$; otherwise decide C_1 (i.e., clear plastic) if $x < 1.3341$; otherwise decide C_2 (i.e., white plastic).

The probability of error for dual-energy measurement by directly using (5.7) is given by,

$$P(error) = 1 - \frac{1}{3}\left[\int_{-\infty}^{1.3341} \frac{1}{\sqrt{2\pi}\sigma_1} e^{-\frac{(x-\mu_1)^2}{2\sigma_1^2}} dx + \int_{1.3341}^{1.5760} \frac{1}{\sqrt{2\pi}\sigma_2} e^{-\frac{(x-\mu_2)^2}{2\sigma_2^2}} dx + \int_{1.5760}^{\infty} \frac{1}{\sqrt{2\pi}\sigma_3} e^{-\frac{(x-\mu_3)^2}{2\sigma_3^2}} dx\right] = 10.4\% \tag{5.32}$$

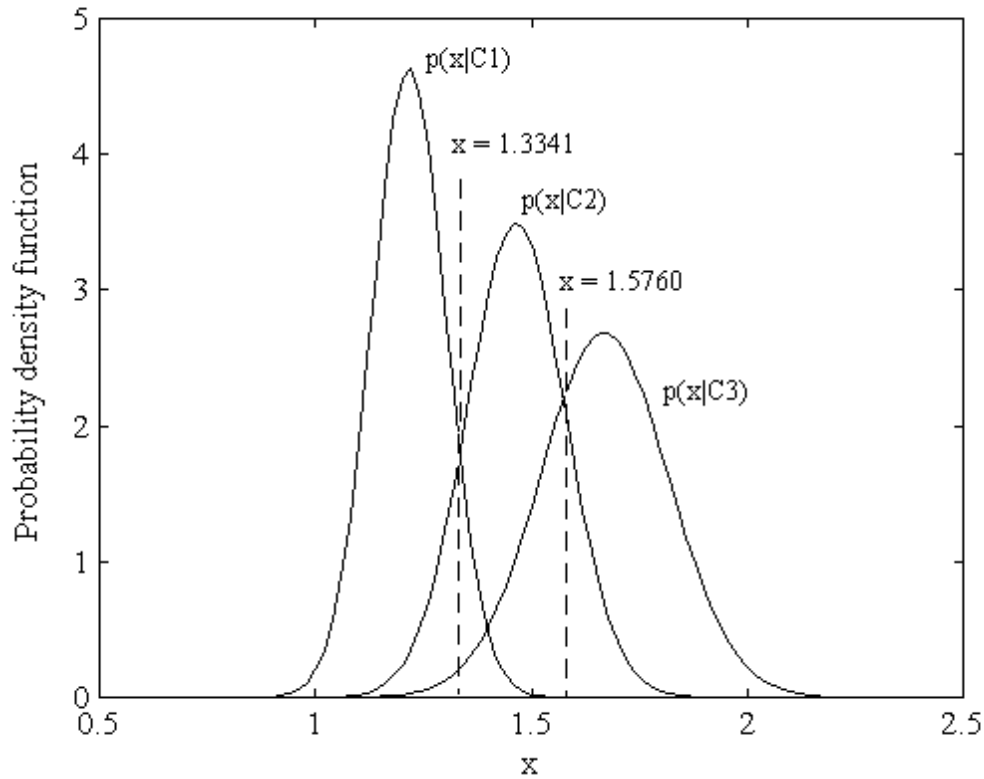

Figure 5.5-1 Estimated probability density functions of three dual-energy classes and the discriminant boundaries for three step wedges.

The probability density function of dual-energy by using Algorithm 5.1 and the discriminant boundaries for three step wedges are shown in Figure 5.5-2. The rule, which was obtained in similar method as the previous one, is as follows: decide C_3 (i.e., aluminum) if $x > 1.1650$; otherwise decide C_1 (i.e., clear plastic) if $x < 2.0$; otherwise decide C_2 (i.e., white plastic).

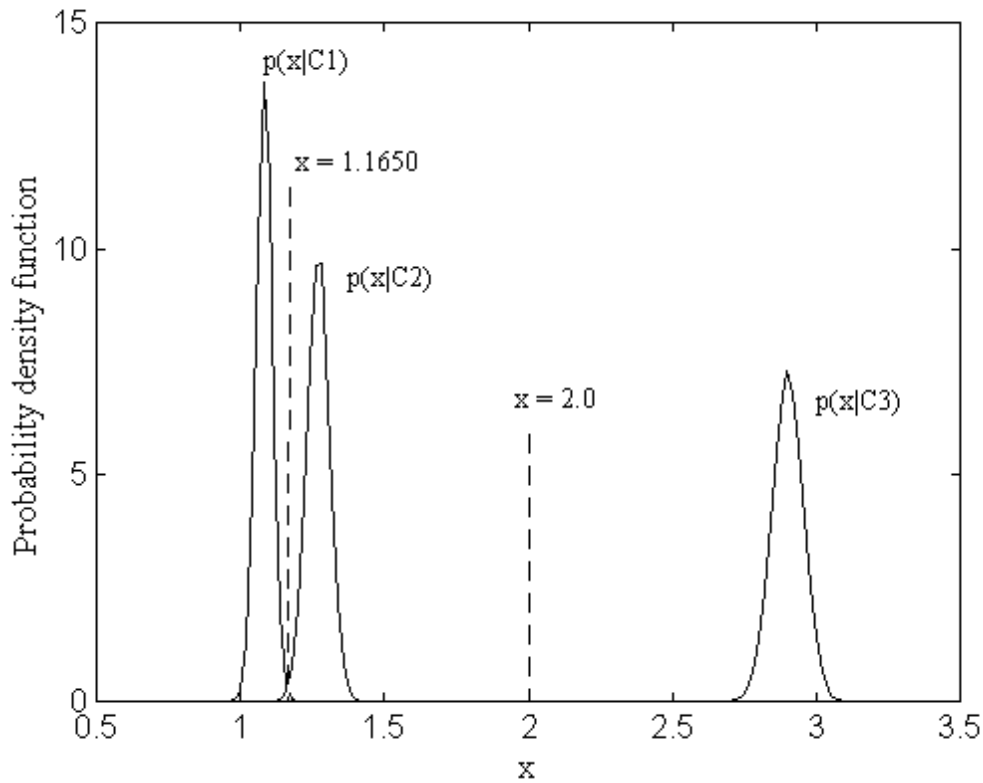

Figure 5.5-2 Estimated probability density functions of dual-energy measurements and the discriminant boundaries for three step wedges.

The probability of error for dual-energy measurements by using the numerical optimization method is therefore given by,

$$P(error) = 1 - \frac{1}{3}\left[\int_{-\infty}^{1.1650} \frac{1}{\sqrt{2\pi}\sigma_1} e^{-\frac{(x-\mu_1)^2}{2\sigma_1^2}} dx + \int_{1.1650}^{2.0} \frac{1}{\sqrt{2\pi}\sigma_2} e^{-\frac{(x-\mu_2)^2}{2\sigma_2^2}} dx + \int_{2.0}^{\infty} \frac{1}{\sqrt{2\pi}\sigma_3} e^{-\frac{(x-\mu_3)^2}{2\sigma_3^2}} dx\right] = 0.3\% \tag{5.33}$$

From (5.32) and (5.33), it can be seen that comparing with dual-energy measurements by directly using Equation (5.7), dual-energy by using the numerical optimization method has a lower probability of error for three step wedges. It means that numerical optimization can improve materials characterization by decreasing the error rate. The comparison is done with three material types, but a similar analysis should yield similar results for an arbitrary set of materials.